Flip-OFDM for Unipolar Communication Systems

Nirmal Fernando, *Student Member, IEEE,* Yi Hong, *Senior Member, IEEE,* and Emanuele Viterbo, *Fellow, IEEE*

***Abstract*—Unipolar communications systems can transmit information using only real and positive signals. This includes a variety of physical channels ranging from optical (fiber or free-space), to RF wireless using amplitude modulation with non-coherent reception, to baseband single wire communications. Unipolar OFDM techniques can efficiently compensate frequency selective channel distortion in unipolar communication systems. One of the leading example of unipolar OFDM is asymmetric clipped optical OFDM (ACO-OFDM) originally proposed for optical communications. Flip-OFDM is an alternative approach that was proposed in a patent, but its performance and full potentials have never been investigated in the literature. In this paper, we first compare Flip-OFDM and ACO-OFDM, and show that both techniques have the same performance but different complexities. In particular, Flip-OFDM offers 50% saving in hardware complexity at the receiver over ACO-OFDM. We then propose a new detection scheme, which enables to reduce the noise at the Flip-OFDM receiver by almost 3dB. The analytical performance of the noise filtering schemes is supported by the simulation results.**

***Index Terms*—OFDM, detection, non-coherent communications, optical communications, unipolar baseband communications.**

I. Introduction

UNIPOLAR communications systems can transmit information using only *real* and *positive* signals. Common examples of unipolar communication systems include optical communications (fiber and free space) [1], [2], amplitude modulated RF wireless communications, and baseband digital communications over a single wire [3]. Channel dispersion or multipath fading may cause the inter-symbol-interference and degrade the performance of such unipolar communication systems. To compensate for these effects, unipolar orthogonal frequency division multiplexing (OFDM) can be used. The two most popular unipolar OFDM techniques are DC-offset OFDM (DCO-OFDM) [2] and Asymmetrically clipped optical OFDM (ACO-OFDM) [5]. However, an alternative approach (hereafter denoted by Flip-OFDM) was proposed in a patent [12], but its performance has never been analyzed nor compared with the other unipolar techniques.

The principles of the main unipolar OFDM techniques are described below:

- DC-offset OFDM (DCO-OFDM) [2], known as the traditional unipolar OFDM technique, uses the Hermitian symmetry property with a DC-bias to generate a *real* and *positive* time domain signal. However, the DC bias depends on the peak-to-average-power ratio (PAPR) of the OFDM symbol. Since OFDM has a high PAPR, the amplitude of the DC bias is generally significant. It was shown in [4] that the requirement of large DC-bias makes DCO-OFDM optically power inefficient. Conversely, the use of lower DC bias can lead to frequent clipping of the negative parts of the time-domain signal. This can cause inter-carrier interference and create out-of-band optical power.
- Asymmetrically clipped optical OFDM (ACO-OFDM) was proposed in [5] and does not require any DC bias. ACO-OFDM only uses odd subcarriers to transmit information symbols, and the negative part of the time-domain signal is clipped. It was shown in [5] that this clipping does not distort information symbols in odd subcarriers, although their amplitudes are scaled by half. In [4], [6], [7], the performance of ACO-OFDM was compared to other modulation schemes such as on-off keying and DC-biased OFDM (DC-OFDM); and it was shown that ACO-OFDM has better power efficiency over optical wireless channels [4]. Performance of ACO-OFDM can be further improved by using bit loading and diversity combining schemes, as discussed in [8], [9], [10]. Different from the above comparison over optical wireless channels, in [11], the power efficiency comparison between ACO-OFDM, on-off keying, and DC-OFDM are presented specifically for single-mode fiber optical communications.
- In Flip-OFDM [12], positive and negative parts are extracted from the real bipolar OFDM symbol generated by preserving the Hermitian symmetry property of transmitted information symbols. Then the polarity of negative parts are inverted before transmission of both positive and negative parts in two consecutive OFDM symbols. Since the transmitted signal is always positive, Flip-OFDM is indeed a unipolar OFDM technique that can be used for unipolar communications.

The main contributions of this paper are:

- A comprehensive analysis of Flip-OFDM in the general setting of unipolar communication systems: we modified the original Flip-OFDM and compared the key system parameters with ACO-OFDM, including spectral efficiency, bit error rate (BER) performance and complexity.
- A new detection enhancement scheme for Flip-OFDM: we show both analytically and by simulations that a significant BER improvement can be achieved with a simple time-domain noise filtering technique at receiver.

The rest of the paper is organized as follows. In Section II, we define the unipolar communication systems that can be benefited from unipolar OFDM techniques. In Section III, we introduce Flip-OFDM and ACO-OFDM and compare

Paper approved by H. Arslan, the Editor for Cognitive Radio and OFDM of the IEEE Communications Society. Manuscript received December 13, 2011; revised April 8, 2012.

The authors are with the Department of Electrical and Computer System Engineering, Monash University, Clayton, VIC 3800, Australia (e-mail: {Nirmal.Fernando, Yi.Hong, Emanuele.Viterbo}@monash.edu).

Digital Object Identifier 10.1109/TCOMM.2012.082712.110812

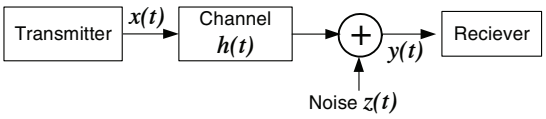

Fig. 1. Equivalent model for unipolar communication system.

their key system parameters including spectral efficiencies, BER performance and hardware complexities. In Section IV, we propose a new detection scheme for Flip-OFDM. We also analyze the performance of Flip-OFDM using the new detection scheme. Finally, conclusions are drawn in Section V.

II. Unipolar communication model

A communication system can be modeled as a linear baseband equivalent system, as shown in Fig. 1. Let $x(t)$, $h(t)$ and $z(t)$ represent the transmit signal (e.g. an intensity or amplitude signal), the channel impulse response, and the noise component, respectively. Then the communication is said to be unipolar if the following two conditions are satisfied:

1) $x(t)$ is real and $x(t) \geq 0$ for all t.
2) if the equivalent received signal $y(t)$ can be modeled as

$$y(t) = h(t) \otimes x(t) + z(t) \tag{1}$$

where $\otimes$ represents convolution, $h(t) \geq 0$ for all t and $z(t)$ is Gaussian noise with zero mean and power σ_z^2.

If the channel is normalized such that $\int_{-\infty}^{+\infty} |h(t)|^2 \, dt = 1$, then the *equivalent signal-to-noise ratio* (SNR) is defined as

$$\text{SNR} = \frac{E[x^2(t)]}{\sigma_z^2} \tag{2}$$

where $E[\cdot]$ is the expectation operator.

Note that such an equivalent baseband model can represent the process of modulation and demodulation of bandpass signals transmitted over the physical channels. Common examples for such unipolar communication systems are:

- *Optical communications (fiber or free space)* – The unipolar information carrying signal $x(t)$ modulates the optical intensity of an LED or a laser. Since the intensity can not be negative and the photodetector can not recover the phase of the optical carrier at the receiver, the equivalent optical channel can be modeled with a unipolar $h(t)$ [1], [13], [14].
- *Amplitude Modulated RF Wireless* – In a typical RF communication, the information is transferred through the amplitude and phase of a carrier signal. At the receiver, complex baseband processing is necessary to recover the phase information. In amplitude modulated RF wireless, only amplitude modulation with a unipolar modulating signal can be used. Hence, the simple envelope detection can be used at the receiver so that the equivalent channel can be modeled with a unipolar $h(t)$.
- *Baseband digital communication* – A baseband system transmitting data over a single wire (e.g. TTL logic [3]) can only use positive signals (e.g. unipolar NRZ [3]). The channel can be modeled with an unipolar $h(t)$.

III. Unipolar OFDM Techniques

In this section, we compare Flip-OFDM and ACO-OFDM in the general setting of unipolar communication systems.

A. Flip-OFDM

A block diagram of a Flip-OFDM transmitter is shown in Fig. 2(a). Let X_n be the transmitted QAM symbol in the n-th OFDM subcarrier. The output of the Inverse Fast Fourier Transform (IFFT) operation at the k-th time instant is given by

$$x[k] = \sum_{n=0}^{N-1} X_n \exp\left(\frac{j2\pi nk}{N}\right) \tag{3}$$

where N is the IFFT size and $j^2 = -1$. If the symbol X_n transmitted over each OFDM subcarrier is independent, the time-domain signal $x[k]$ produced by the IFFT operation is complex. A real signal can be then obtained by imposing the Hermitian symmetry property

$$X_n = X_{N-n}^*, \quad n = 0, 1, 2..., N/2 - 1 \tag{4}$$

where * denotes complex conjugation. This property implies that half of the OFDM subcarriers are sacrificed to generate the real time-domain signal. The output of IFFT operation in (3) can be rewritten as

$$\begin{aligned} x[k] &= X_0 + \sum_{n=1}^{N/2-1} X_n \exp\left(\frac{j2\pi nk}{N}\right) + X_{N/2} \exp\left(j\pi k\right) \\ &+ \sum_{n=N/2+1}^{N-1} X_{N-n}^* \exp\left(\frac{j2\pi nk}{N}\right) \end{aligned} \tag{5}$$

where X_0 is the DC component. To avoid any DC shift or any residual complex component in the time domain signal, we let

$$X_0 = X_{N/2} = 0.$$

In such a way, the output of the IFFT operation is a real signal, but not yet unipolar. We can then decompose this signal as

$$x[k] = x^+[k] + x^-[k]$$

where the positive and negative parts are defined as

$$\begin{aligned} x^+[k] &= \begin{cases} x[k] & \text{if } x[k] \geq 0 \\ 0 & \text{otherwise} \end{cases} \\ x^-[k] &= \begin{cases} x[k] & \text{if } x[k] < 0 \\ 0 & \text{otherwise} \end{cases} \end{aligned} \tag{6}$$

and $k = 1, 2, ..., N$. These two components are separately transmitted over two successive OFDM symbols. The positive signal $x^+[k]$ is transmitted in the first subframe (positive subframe), while the flipped (inverted polarity) signal $-x^-[k]$ is transmitted in the second subframe (negative subframe). Since the transmission is over a frequency selective channel, the cyclic prefixes composed of Δ samples are added to each of the OFDM subframes. Hence, the negative OFDM subframe is delayed by $(N + \Delta)$ and transmitted after the positive subframe.

The reconstruction of the bipolar OFDM frame and the detection process at the receiver are illustrated in Fig. 2(b).

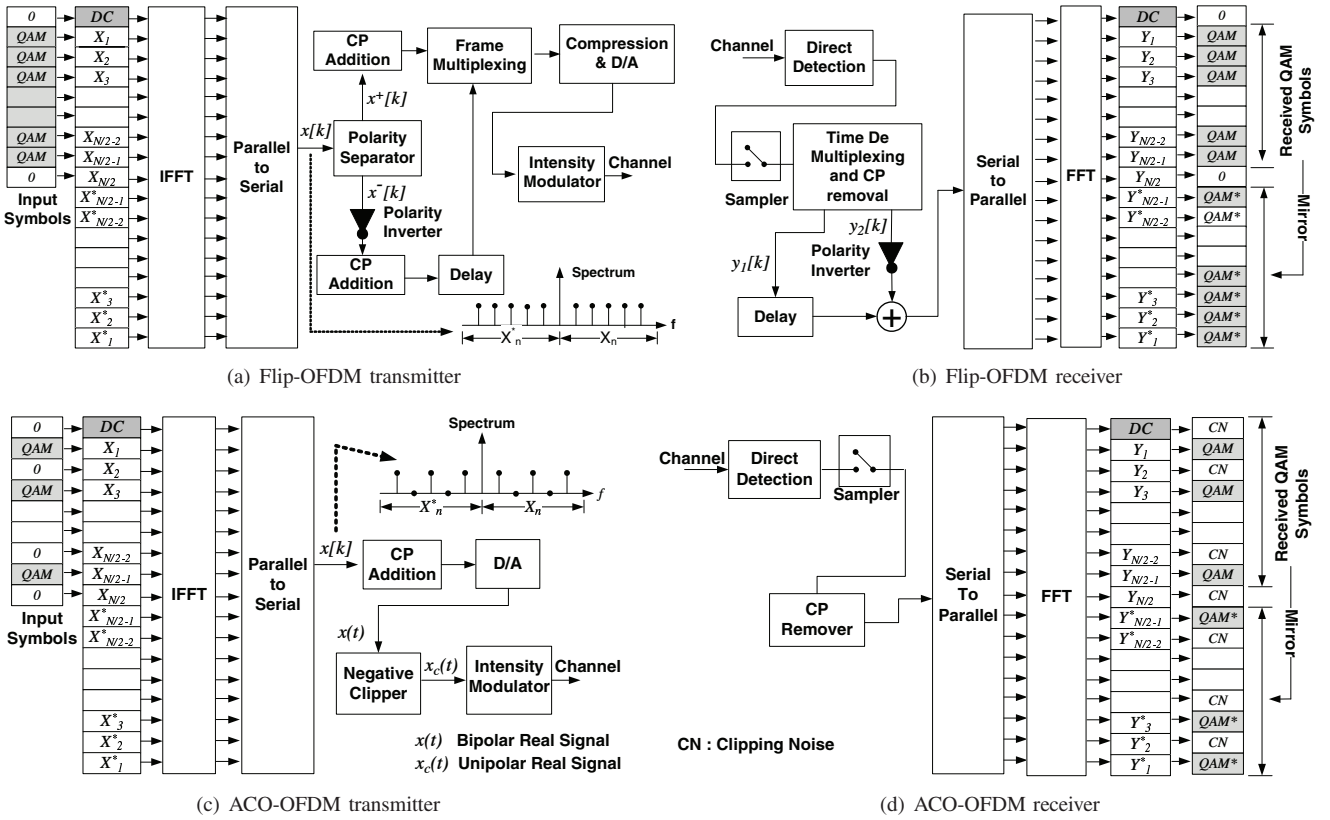

(a) Flip-OFDM transmitter

(b) Flip-OFDM receiver

(c) ACO-OFDM transmitter

(d) ACO-OFDM receiver

Fig. 2. Block Diagrams of Flip-OFDM and ACO-OFDM transmitters and receivers.

The cyclic prefixes associated with each OFDM subframe are removed. Then the original signal is reconstructed as

$$y[k] = y_1[k] - y_2[k] \tag{7}$$

where $y_1[k]$ and $y_2[k]$ represent the time-domain samples received in the positive and negative subframes, respectively. The Fast Fourier Transform (FFT) operation is performed on the bipolar signal to detect the transmitted QAM information symbols.

B. ACO-OFDM

A block diagram of an ACO-OFDM transmitter is shown in Fig. 2(c). At the transmitter, the QAM information symbols are first mapped onto the first half of the odd subcarriers, X_{2n+1}, where $n = 0, 1, 2, ..., N/4 - 1$. The even subcarriers are set to zero, i.e.

$$X_{2n} = 0, \quad n = 0, 1, 2, ..., N/2 \tag{8}$$

Using the above equation, the DC component and the symbol of the $\frac{N}{2}$-th subcarrier become zero. The Hermitian symmetry property in (4) is used to construct a real signal. After the IFFT operation, the time-domain OFDM symbol $x[k]$ can be computed using (5) and has an odd symmetry property

$$x[k] = -x\left[k + \frac{N}{2}\right]. \tag{9}$$

This allows clipping of the negative time samples of $x[k]$ right after the DA conversion at the transmitter without destroying the original information. The clipped signal $x_c(t)$ is a unipolar signal, defined as

$$x_c(t) = \begin{cases} x(t) & \text{if } x(t) \geq 0 \\ 0 & \text{Otherwise.} \end{cases} \tag{10}$$

The cyclic prefix is then added to the clipped unipolar OFDM symbol before the transmission.

The direct detection (DD) of the received signal $y(t)$ is performed at the receiver, as illustrated in Fig. 2(d). The cyclic prefix of the OFDM symbol is removed and the serial-to-parallel conversion is performed. The FFT operation is performed and finally the QAM information symbols contained in the odd subcarriers can be detected.

C. Comparison of Flip-OFDM and ACO-OFDM

For a fair comparison, we assume the same channel model with the same delay spread for both Flip-OFDM and ACO-OFDM.

Modification to Flip-OFDM – The original Flip-OFDM [12] uses compression of time samples to obtain the same duration of a standard bipolar OFDM symbol. The compression requires two half-length cyclic prefixes in each subframe, when compared to that of ACO-OFDM. This results in different capabilities between the two systems to combat delay spread distortion of the channel. Here, we do not compress the time scale and both consecutive OFDM subframes of Flip-OFDM will have the same cyclic prefix as those of ACO-OFDM, as shown in Fig. 3. Hence, our modification guaranties that Flip OFDM occupies the same bandwidth as ACO-OFDM.

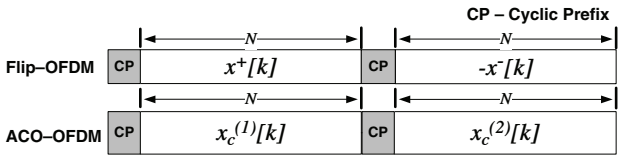

Fig. 3. OFDM symbol structure used to compare Flip-OFDM and ACO-OFDM. We assume FFT and IFFT sizes of both ACO-OFDM and Flip-OFDM are the same. N denotes the FFT and IFFT size for each case.

Spectral Efficiency – In ACO-OFDM, each OFDM symbol (i.e. $x_c^{(1)}$ and $x_c^{(2)}$) carries $N/4$ information symbols. In Flip-OFDM, each symbol carries $\frac{N-2}{2}$ information symbols, (the first and $\frac{N}{2}$-th subcarriers are not used to transmit information symbol). Given that two OFDM subframes are used to transmit all the information symbols, the data rates in both schemes are approximately the same, for sufficiently large N. This guarantees the same spectral efficiencies for both scheme.

Symbol Energy – In Flip-OFDM, the energy E_s of an information symbol is split across the positive and negative OFDM subframes during the flipping process, as shown in Fig. 4(a). The total energy per subframe is $E_s(N-2)/2$ and for sufficiently large N, this is approximately $E_sN/2$.

In order to transmit the same power, the energy in an ACO-OFDM frame and a Flip-OFDM subframe must be the same i.e $E_sN/2$. Hence, the energy of an ACO-OFDM information symbol is set to be $2E_s$ to compensate for the zero odd subcarriers and the fact that clipping discards half of the original signal energy and the remaining part is split evenly among even and odd subcarriers, as illustrated in Fig. 4(b). The energy in the odd subcarriers is known as the *clipping noise* [5], [6].

Noise Power – In Flip-OFDM, the noise power of the Flip-OFDM is doubled during the recombination of the positive and negative OFDM subframes. Let H_n^+ and H_n^- be the channel responses of the n-th OFDM subcarrier over two subframes respectively, the outputs of the n-th OFDM subcarrier in the two subframes are

$$Y_n^+ = H_n^+ X_n^+ + Z_n^+ \quad (11)$$

$$Y_n^- = -H_n^- X_n^- + Z_n^- \quad (12)$$

where Z_n^+ and Z_n^- represent the noise components of the n-th OFDM subcarrier. Under slow fading characteristics, we can assume the channel is constant over two consecutive OFDM symbols (i.e. $H_n^+ = H_n^- \triangleq H_n$). Then the addition of (11) and (12) yields

$$R_n = H_n X_n + \{Z_n^+ + Z_n^-\}. \quad (13)$$

where R_n is the received information symbol. As Z_n^+ and Z_n^- are Gaussian (i.e. $\sim \mathcal{N}(0, \sigma_z^2)$), the noise power of the received information symbols is $2\sigma_z^2$.

In ACO-OFDM, since there is no recombination, the received information symbol is given by

$$R_{2n+1} = \frac{1}{2} H_{2n+1} X_{2n+1} + Z_{2n+1}. \quad (14)$$

and the noise power is σ_z^2, which is half of the amount in Flip-OFDM.

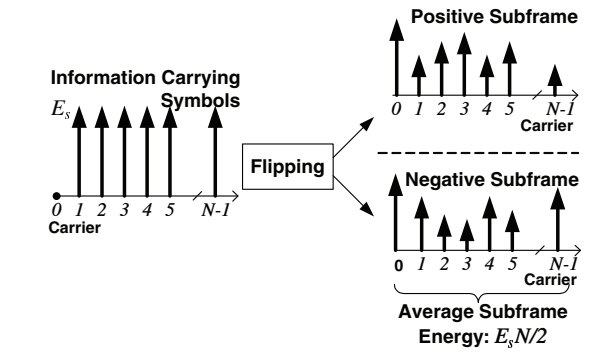

(a)

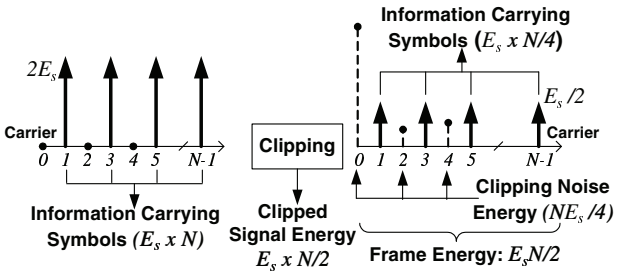

(b)

Fig. 4. Effects on symbol energies in ACO- and Flip-OFDM due to the clipping and flipping processes.

Equivalent SNR – Since half of the transmitted signal energy goes in the even subcarriers in ACO-OFDM and the other half is the clipping noise, the SNRs of both ACO-OFDM and Flip-OFDM are the same. Using (2), the equivalent SNR per received sample is given by

$$\text{SNR} = \frac{\sigma_x^2}{2\sigma_z^2} \quad (15)$$

where σ_x^2 denotes the transmitted signal power.

Bit Error Rates – The analytical BER expression for both Flip-OFDM and ACO-OFDM in AWGN channels can be computed as [3]

$$P_b \simeq \frac{2}{\log_2 M}\left(1 - \frac{1}{\sqrt{M}}\right) \text{ erfc}\left(\sqrt{\frac{3}{2(M-1)}\text{SNR}}\right) \quad (16)$$

for a rectangular *M*-QAM constellation, where erfc$(\cdot)$ is the complementary error function. The simulated BER performance of Flip-OFDM and ACO-OFDM for the specified optical wireless channel having strong LOS signal (Directed, has AWGN characteristics [14]) and multipath propagation signals (Nondirected or Diffused mode), were compared in [15]. Here it was shown that both systems have the same BER performance, which can be accurately predicted by (16).

Complexity – We define complexity as the number of FFT/IFFT operations at the transmitter or the receiver. A complexity comparison is given in Table I. At the transmitter, both schemes have approximately the same complexity for a sufficiently large values of N, assuming that the IFFT operation for ACO-OFDM is optimized using the fact that half of the subcarriers are zero. However, at the receiver, Flip-OFDM offers a 50% complexity saving compared to ACO-OFDM.

TABLE I
COMPLEXITY COMPARISON OF FLIP- AND ACO-OFDMS

	ACO-OFDM	Flip-OFDM
Transmitter	$2\ (\frac{N}{2})\log(\frac{N}{2})$	$N\log(N)$
Receiver	$2N\log(N)$	$N\log(N)$

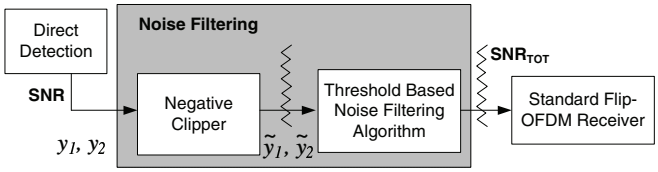

Fig. 5. The stages of noise reduction at the Flip-OFDM receiver.

IV. ENHANCED DETECTION FOR FLIP-OFDM

Assuming the channel has a strong LOS signal (i.e. AWGN), at the receiver, we introduce a new detection scheme including two nonlinear noise filtering stages for the time domain samples, as shown in Fig. 5. In the first stage of the detection, a negative clipper is placed immediately after DD. In the second stage, a threshold based noise filter is used to further improve the BER performance. Then the preprocessed time samples are sent to the FFT operation for the detection procedure.

A. Negative Clipper

In unipolar communications, although the transmitted signal is always positive, the received signal can be negative due to Gaussian noise [1], [13]. Therefore, negative clipper can be used to force the negative sample to be zero. This idea was proposed in [9] for ACO-OFDM; and can be used in our detection as the first stage of noise filtering.

Recall $y_1[k]$ and $y_2[k]$ in (7), i.e., the k-th received time samples of the positive and negative OFDM subframes. For simplicity of notation, we omit the index k in the rest of the paper.

Since positive and negative OFDM subframes are defined with same unipolar OFDM frame, only one sample (y_1 or y_2) must contain the signal component x (x^+ or x^-), i.e. either

$$\begin{aligned} y_1 &= x^+ + z_1 = x + z_1 \\ y_2 &= z_2 \end{aligned} \tag{17}$$

or

$$\begin{aligned} y_1 &= z_1 \\ y_2 &= -x^- + z_2 = x + z_2 \end{aligned} \tag{18}$$

where $z_1, z_2 \sim \mathcal{N}(0, \sigma_z^2)$. For large IFFT sizes, the output produced by the IFFT operation is i.i.d and has a Gaussian distribution ($\sim \mathcal{N}(0, \sigma_x^2)$). Hence, the pdf of the x is a one sided Gaussian

$$f_X(x) = \begin{cases} 0 & x < 0 \\ \sqrt{\frac{2}{\pi\sigma_x^2}}\exp\left(-\frac{x^2}{2\sigma_x^2}\right) & x \geq 0. \end{cases} \tag{19}$$

We see that y_1 and y_2 can be negative since both z_1 and z_2 in (17) and (18) have double sided Gaussian distributions. The clipping process at the negative clipper is given by

$$\tilde{y}_1 = [y_1]^+ \triangleq \begin{cases} y_1 & \text{if } y_1 \geq 0 \\ 0 & \text{otherwise} \end{cases} \tag{20}$$

$$\tilde{y}_2 = [y_2]^- \triangleq \begin{cases} y_2 & \text{if } y_2 \geq 0 \\ 0 & \text{otherwise.} \end{cases} \tag{21}$$

Since x is equal likely to appear in y_1 and y_2, for simplicity, we assume x appears in y_1 only. For a given x, the equivalent noise power $\sigma_{\text{NC}}^2(x)$ can be computed as

$$\begin{aligned} \sigma_{\text{NC}}^2(x) &= \frac{1}{2}E\left[(\tilde{y}_1 - \tilde{y}_2 - x)^2\right] \\ &= \frac{1}{2}E\left[(\tilde{y}_1 - x)^2\right] + \frac{\sigma_z^2}{4} - \frac{\sigma_z}{\sqrt{2\pi}}E\left[\tilde{y}_1 - x\right] \end{aligned} \tag{22}$$

where

$$\begin{aligned} E[(\tilde{y}_1 - x)^2] &= \frac{(x^2 - \sigma_z^2)}{2}\text{erfc}\left(\frac{x}{\sqrt{2}\sigma_z}\right) - \frac{x\sigma_z e^{-\frac{x^2}{2\sigma_z^2}}}{\sqrt{2\pi}} + \sigma_z^2 \\ E[\tilde{y}_1 - x] &= \frac{\sigma_z e^{-\frac{x^2}{2\sigma_z^2}}}{\sqrt{2\pi}} - \frac{x}{2}\text{erfc}\left(\frac{x}{\sqrt{2}\sigma_z}\right) \end{aligned}$$

because $\tilde{y}_1$ and $\tilde{y}_2$ are independent. Since $\sigma_{\text{NC}}^2(x)$ is conditioned by x, we can estimate σ_{NC}^2 using

$$\begin{aligned} \sigma_{\text{NC}}^2 &= \int_0^\infty \sigma_{\text{NC}}^2(x) f_X(x)\, dx \\ &= \frac{{\sigma_z}^2}{2} + \frac{-\sigma_z\sqrt{{\sigma_z}^2 + {\sigma_x}^2} + ({\sigma_z}^2 + {\sigma_x}^2)\tan^{-1}\left(\frac{\sigma_z}{\sigma_x}\right)}{2\pi} \end{aligned} \tag{23}$$

Similarly, when x contributes to $\tilde{y}_2$, we simply obtain the same σ_{NC}^2 in (23). Hence, the total equivalent noise after negative clipping is given in (23) and the improved equivalent SNR per sample is

$$\text{SNR}_{\text{NC}} = \frac{E[x^2]}{\sigma_{\text{NC}}^2} = \frac{\sigma_x^2}{2\sigma_{\text{NC}}^2} \tag{24}$$

Substituting SNR_{NC} to (16) yields the new theoretical BER performance at the first stage of noise filtering.

B. Threshold Based Noise Filtering Algorithm

Without loss of generality, we assume that the signal component x is only contained in y_1, as in (20), since the following development can be easily applied to the dual case (i.e., x is only contained in y_2, as in (21)).

Under this assumption, after the first stage of noise filtering (negative clipper), we have

$$\tilde{y}_1 = [x + z_1(x)]^+ = x + \tilde{z}_1(x) \tag{25}$$

$$\tilde{y}_2 = [z_2]^+ = \tilde{z}_2 \tag{26}$$

where $\tilde{z}_1(x)$ and $\tilde{z}_2$ are the additive noise components after the negative clipper, and the $[\cdot]^+$ operator is defined in (20). Let $\tilde{y}$ be the reconstructed bipolar OFDM sample given by

$$\begin{aligned} \tilde{y} &\triangleq \tilde{y}_1 - \tilde{y}_2 \\ &= [x + z_1(x)]^+ - [z_2]^+ \quad (27) \\ &= x + \tilde{z}_1(x) - \tilde{z}_2 \quad (28) \end{aligned}$$

We notice that $\tilde{z}_1(x)$ has a dependency on x as a result of the negative clipping. Since x is always positive, there is

TABLE II
THRESHOLD BASED ALGORITHM OUTPUTS

Case		Outputs ($\tilde{y}$)
A	$\lvert\tilde{y}_1 - \tilde{y}_2\rvert \le c$	$\tilde{y}_1 - \tilde{y}_2 = x + \tilde{z}_1(x) - \tilde{z}_2$
B	$\tilde{y}_1 - \tilde{y}_2 > c$	$\tilde{y}_1 = x + \tilde{z}_1(x)$
C	$\tilde{y}_2 - \tilde{y}_1 > c$	$\tilde{y}_2 = \tilde{z}_2$

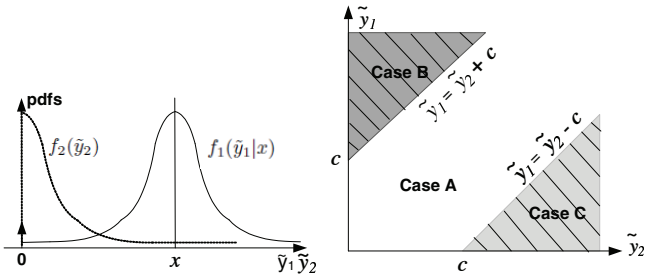

(a) (b)

Fig. 6. (a) Distributions of $\tilde{y}_1$ and $\tilde{y}_2$ if x is fixed; (b) operation regions of the threshold based noise reduction algorithm.

a higher likelihood that the signal sample $\tilde{y}_1$ containing x is greater than the pure noise sample $\tilde{y}_2$. Ideally, if we can perfectly identify the signal sample $\tilde{y}_1$, we can simply ignore the sample containing any noise, i.e., we set $\tilde{y}_2$ to 0. Hence, at the receiver, the binary decision is made by looking at the difference between $\tilde{y}_1$ and $\tilde{y}_2$, relative to a threshold c. All the possible outcomes are shown in Table II. In Case A, the difference $|\tilde{y}_1 - \tilde{y}_2|$ is below the threshold, so that both $\tilde{z}_1(x)$ and $\tilde{z}_2$ contribute to the overall noise power of the output sample $\tilde{y} = \tilde{y}_1 - \tilde{y}_2$. Case B corresponds to the ideal case discussed above and the output $\tilde{y} = \tilde{y}_1$ has a significantly reduced noise power. Case C is the least frequent but will cause a completely wrong estimation of x. In all cases an incorrect decision may not only destroy the signal, but also increase the noise power. The corresponding algorithm is given below.

Algorithm 1 : Threshold based noise reduction algorithm

Input $\tilde{y}_1$, $\tilde{y}_2$, c
if $\tilde{y}_1 - \tilde{y}_2 > c$ **then**
  $\tilde{y}_2 \leftarrow 0$
else if $\tilde{y}_2 - \tilde{y}_1 > c$ **then**
  $\tilde{y}_1 \leftarrow 0$
end if
Output $\tilde{y} = \tilde{y}_1 - \tilde{y}_2$

We observe that the probability of each of the three cases depends on x and the threshold c. In the next section, we will compute the optimal threshold to achieve the best possible BER performance of Flip-OFDM.

C. Design of the optimal threshold and performance analysis

The objective of the threshold base noise filtering algorithm is to minimize the overall noise power by tuning the threshold c. The algorithm differs from standard detection algorithms due to three main reasons: (*i*) x is not fixed and has a single sided Gaussian distribution, as given in (19); (*ii*) $\tilde{z}_1(x)$ and $\tilde{z}_2$ are not Gaussian random variables since they are clipped by the negative clipper; and (*iii*) $\tilde{z}_1(x)$ distribution depends on the random variable x. In order to simplify the analysis, we first fix x, as shown in Fig. 6, and find the equivalent noise power conditioned on x. That is, given x, the pdfs of $\tilde{y}_1$ and $\tilde{y}_2$ are

$$f_1(\tilde{y}_1|x) = \begin{cases} \frac{\delta(\tilde{y}_1)}{2}\text{erfc}\left(\frac{x}{\sqrt{2}\sigma_z}\right) & \text{if } \tilde{y}_1 = 0 \\ \frac{1}{\sqrt{2\pi}\sigma_z}\exp\left(-\frac{(\tilde{y}_1 - x)^2}{2\sigma_z^2}\right) & \text{if } \tilde{y}_1 > 0 \end{cases} \quad (29)$$

$$f_2(\tilde{y}_2) = \begin{cases} \frac{\delta(\tilde{y}_2)}{2} & \text{if } \tilde{y}_2 = 0 \\ \frac{1}{\sqrt{2\pi}\sigma_z}\exp\left(-\frac{\tilde{y}_2^2}{2\sigma_z^2}\right) & \text{if } \tilde{y}_2 > 0 \end{cases} \quad (30)$$

where $f_1(\tilde{y}_1|x)$ is a function of x. Let $\sigma^2_{\text{A}}(c,\sigma_z,x)$, $\sigma^2_{\text{B}}(c,\sigma_z,x)$ and $\sigma^2_{\text{C}}(c,\sigma_z,x)$ be the noise powers of Case A, B and C for a given x. Since $\tilde{y}_1$ and $\tilde{y}_2$ are independent, we obtain

$$\begin{aligned}
\sigma^2_{\text{A}}(c,\sigma_z,x) &= \int_0^c \mathrm{d}\tilde{y}_1 \int_0^{\tilde{y}_1+c} (\tilde{y}_1 - \tilde{y}_2 - x)^2 f_1(\tilde{y}_1|x) f_2(\tilde{y}_2)\,\mathrm{d}\tilde{y}_2 \\
&\quad + \int_c^\infty \mathrm{d}\tilde{y}_1 \int_{\tilde{y}_1-c}^{\tilde{y}_1+c} (\tilde{y}_1 - \tilde{y}_2 - x)^2 f_1(\tilde{y}_1|x) f_2(\tilde{y}_2)\,\mathrm{d}\tilde{y}_2 \\
\sigma^2_{\text{B}}(c,\sigma_z,x) &= \int_c^\infty \mathrm{d}\tilde{y}_1 \int_0^{\tilde{y}_1-c} (\tilde{y}_1 - x)^2 f_1(\tilde{y}_1|x) f_2(\tilde{y}_2)\,\mathrm{d}\tilde{y}_2 \\
\sigma^2_{\text{C}}(c,\sigma_z,x) &= \int_0^\infty \mathrm{d}\tilde{y}_1 \int_{\tilde{y}_1+c}^\infty (\tilde{y}_2 + x)^2 f_1(\tilde{y}_1|x) f_2(\tilde{y}_2)\,\mathrm{d}\tilde{y}_2
\end{aligned} \quad (31)$$

as shown in Fig. 6(a). The addition of the individual noise contribution in each case corresponds to the average noise power of two time samples. Hence, the average noise power per sample $\sigma^2_{\text{eq}}(c,\sigma_z,x)$ can be given as

$$\sigma^2_{\text{eq}}(c,\sigma_z,x) = \frac{\sigma^2_{\text{A}}(c,\sigma_z,x) + \sigma^2_{\text{B}}(c,\sigma_z,x) + \sigma^2_{\text{C}}(c,\sigma_z,x)}{2}$$

and it is a function of x. Averaging over x, $\sigma^2_{\text{eq}}(c,\sigma_z,x)$ can be estimated as

$$\sigma^2_{\text{eq}}(c,\sigma_z,\sigma_x) = \int_0^\infty \sigma^2_{\text{eq}}(c,\sigma_z,x) f_X(x)\,dx. \quad (32)$$

where $f_X(x)$ is given in (19). The optimum c, denoted by c_{opt}, can be selected such that

$$\frac{\partial \sigma^2_{\text{eq}}(c,\sigma_z,\sigma_x)}{\partial c} = 0. \quad (33)$$

We can use numerical techniques to solve (33) to find c_{opt}. Fig. 7 shows the variation of the normalized c_{opt} with SNR in (15). We see that, when SNR < 4.5dB, c_{opt} is infinite and the algorithm does not bring any gain. In such a case, we have

$$\lim_{c\to\infty} \sigma^2_{\text{eq}}(c,\sigma_z,\sigma_x) = \sigma^2_{\text{NC}} \quad (34)$$

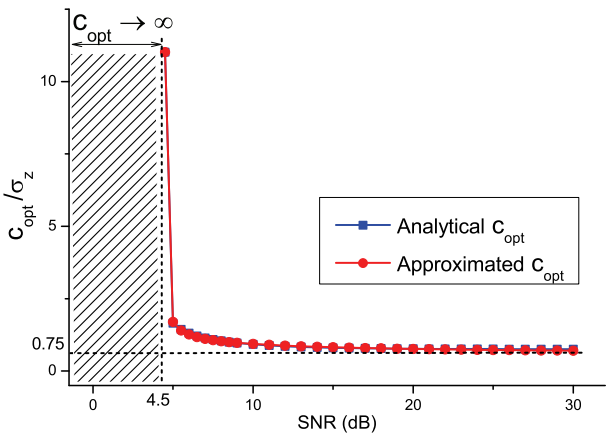

Fig. 7. The variation of the theoretical optimum c (c_{opt}) and approximated optimum c ($\tilde{c}_{\text{opt}}$) with electrical SNR at the receiver. c_{opt} and $\tilde{c}_{\text{opt}}$ are normalized with the standard deviation of the noise power.

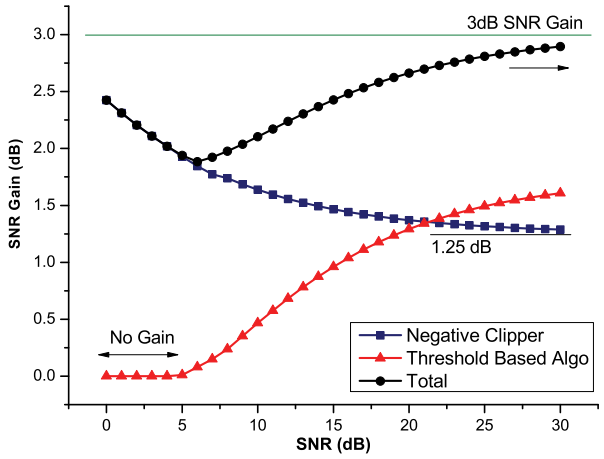

Fig. 8. The SNR gains of the negative clipper and the threshold based noise filtering algorithm with electrical SNR at the receiver.

where σ^2_{NC} is given in (23). When SNR > 4.5dB, c_{opt} is finite and there is a significant SNR gain. Hence, the new SNR can be computed as

$$\text{SNR}_{\text{TOT}} \simeq \frac{\sigma_x^2}{\sigma^2_{\text{eq}}(c_{\text{opt}}, \sigma_z, \sigma_x)}. \tag{35}$$

Since c_{opt} only depends on SNR, we can approximate it as a function of SNR. Using a curve-fitting technique, we can approximate c_{opt} using the following function

$$\tilde{c}_{\text{opt}}/\sigma_z = 0.75\frac{((\text{SNR} - 4.5)^n + a)}{((\text{SNR} - 4.5)^m + b)} \tag{36}$$

where $(a, b, m, n) = (0.9336, 0.03341, 0.4875, 0.3982)$.

We observe from (29) and (30) that the noise after the negative clipper and the algorithm is no longer Gaussian. For a large N, the FFT operation has the effect of whitening the noise in the frequency domain. Hence, the theoretical BER expression in (16) is still valid, given SNRs in (24) and (35) for the respective noise filtering stages.

In the following simulation results we assume $N = 256$. The SNR gains from (i) the negative clipper, (ii) the algorithm, and (iii) both the negative clipper and the algorithm are shown in Fig. 8, respectively. The majority of the gain at low SNR ($<$ 4.5 dB) is contributed by the negative clipper only. However, the gain from the negative clipper reduces as SNR increases; and remains at about 1.25dB at higher SNR ($20 - 30$dB). In contrast, the SNR gain from the algorithm increases steadily as SNR increases. At low SNRs, the negative clipper and the algorithm jointly improve the performance by 1.8-2.5 dB as SNR goes from 0 to 10 dB. At higher SNRs ($10 - 30$dB), the overall SNR gain from both negative clipper and the algorithm ranges from 2.2 to 3dB. The asymptotic 3dB performance gain can be intuitively explained by the fact that, at high SNR, the sample containing the signal component (i.e. $\tilde{y}_1$ or $\tilde{y}_2$), is correctly selected, hence half of the noise power is rejected.

In Fig. 9, we compare both the simulated BER performance and the theoretical one at each noise filtering stage, where 16-QAM signalling is used at the transmitter. As seen in Figs. 8 and 9, the SNR gains in Fig. 8 are accurately reflected in the BER curves. We see that, using the negative clipper and the proposed algorithm, the system has 2.5dB gain at BER of 10^{-4}, when compared to the original system.

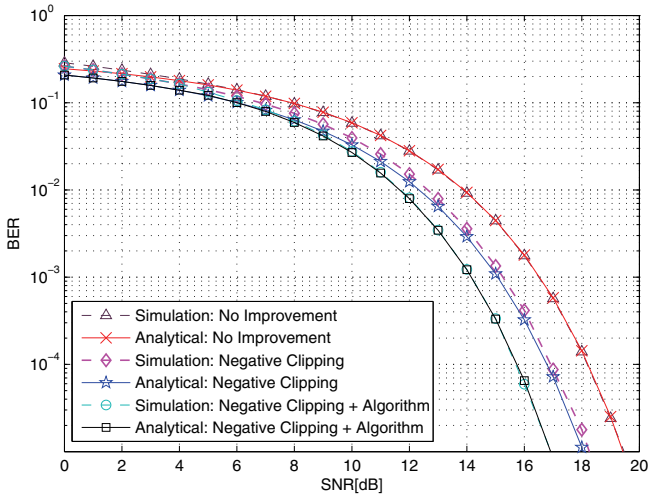

Fig. 9. The improvements of BER performances (16-QAM) due to the negative clipper and the threshold based noise filtering algorithm (N =256).

V. Conclusion

We have analyzed a unipolar OFDM technique (Flip-OFDM) for unipolar communication systems. We showed that it is equivalent to the well-known ACO-OFDM in terms of spectral efficiency and error performance, but can save nearly 50% of receiver complexity over ACO-OFDM. Moreover, we proposed a noise filtering algorithm operating after the negative clipper at the receiver. Both negative clipper and the noise filtering algorithm can jointly contribute up to 3dB gain at high SNR. We note that the noise filtering algorithm can also be applied to ACO-OFDM by comparing the $x[k]$ and $x[k + N/2]$ samples. We expect a similar performance gain to Flip OFDM. Thus, Flip-OFDM is an alternative and efficient unipolar OFDM technique which has potential applications in unipolar communication.

ACKNOWLEDGMENT

This work was performed within the Monash Software Defined Telecommunications Lab and supported by the Monash Professional Fellowship 2011.

REFERENCES

[1] J. Kahn and J. Barry, "Wireless infrared communications," *Proc. IEEE*, vol. 85, no. 2, pp. 265–298, 1997.
[2] J. Armstrong, "OFDM for optical communications," *J. Lightwave Technol.*, vol. 27, no. 3, pp. 189–204, Feb. 2009.
[3] J. G. Proakis, *Digital Communications*, 4th edition. McGraw-Hill, 2001.
[4] J. Armstrong and B. Schmidt, "Comparison of asymmetrically clipped optical OFDM and DC-Biased optical OFDM in AWGN," *IEEE Commun. Lett.*, vol. 12, no. 5, pp. 343–345, May 2008.
[5] J. Armstrong and A. Lowery, "Power efficient optical OFDM," *Electron. Lett.*, vol. 42, no. 6, pp. 370–372, Mar. 2006.
[6] J. Armstrong, B. Schmidt, D. Kalra, H. Suraweera, and A. Lowery, "Performance of asymmetrically clipped optical OFDM in AWGN for an intensity modulated direct detection system," in *Proc. 2006 IEEE Global Telecommun. Conf.*, pp. 1–5.
[7] X. Li, R. Mardling, and J. Armstrong, "Channel capacity of IM/DD optical communication systems and of ACO-OFDM," in *Proc. 2007 IEEE International Conf. Commun.*, pp. 2128–2133.
[8] S. Wilson and J. Armstrong, "Digital modulation techniques for optical Asymmetrically-Clipped OFDM," in *Proc. 2008 IEEE Wireless Commun. Netw. Conf.*, pp. 538–542.
[9] S. Wilson and J. Armstrong, "Transmitter and receiver methods for improving asymmetrically-clipped optical OFDM," *IEEE Trans. Wireless Commun.*, vol. 8, no. 9, pp. 4561–4567, Sep. 2009.
[10] L. Chen, B. Krongold, and J. Evans, "Diversity combining for asymmetrically clipped optical OFDM in IM/DD channels," in *Proc. 2009 IEEE Global Telecommun. Conf.*, pp. 1–6.
[11] D. J. F. Barros and J. M. Kahn, "Comparison of orthogonal frequency-division multiplexing and ONOFF keying in direct-detection multimode fiber links," *J. Lightwave Technol.*, vol. 29, no. 15, pp. 2299–2309, Aug. 2011.
[12] J. Yong, "Modulation and demodulation apparatuses and methods for wired / wireless communication," Korea Patent WO2007/064 165 A, 07, 2007.
[13] J. Carruthers and J. Kahn, "Modeling of nondirected wireless infrared channels," *IEEE Trans. Commun.*, vol. 45, no. 10, pp. 1260–1268, Oct. 1997.
[14] V. Jungnickel, V. Pohl, S. Nonnig, and C. von Helmolt, "A physical model of the wireless infrared communication channel," *IEEE J. Sel. Areas Commun.*, vol. 20, no. 3, pp. 631–640, Apr. 2002.
[15] N. Fernando, Y. Hong, and E. Viterbo, "Flip-OFDM for optical wireless communications," in *2011 IEEE Inf. Theory Workshop*.

Nirmal Fernando received the B.Sc (Hones), and PG. Dip degrees from the Department of Electronic and Telecommunication Engineering, University of Moratuwa, Sri Lanka, in 2009 and 2009, respectively.

He is currently working towards the Ph.D. degree at the Department of Electrical and Computer Systems Eng., at Monash University, Melbourne, Australia. From 2009 to 2010, he has been working as a lecturer at University of Moratuwa, Sri Lanka, from 2006 to 2009, as an Engineer in Dialog Telekom, Sri Lanka. His research interests include non-coherent OFDM techniques, low complexity RF receivers, Optical OFDM, MIMO precoding, signal processing in wireless communications and communication theory.

Yi Hong is currently a lecturer at the Department of Elecectrical and Computer Systems Eng., at Monash University, Melbourne, Australia. She received her Ph.D. degree in Electrical Engineering and Telecommunications from the University of New South Wales (UNSW), Sydney, Australia, in Oct. 2004. She then worked at the Institute of Telecom. Research, University of South Australia, Australia; at the Institute of Advanced Telecom., Swansea University, UK; and at University of Calabria, Italy.

During her PhD, she received an International Postgraduate Research Scholarship (IPRS) from the Commonwealth of Australia; a supplementary Engineering Award from the School of Electrical Engineering and Telecommunications, UNSW; and a Wireless Data Communication System Scholarship from UNSW. She received the NICTA-ACoRN Earlier Career Researcher award for a paper presented at the Australian Communication Theory Workshop (AUSCTW), Adelaide, Australia, 2007.

Dr. Hong is an Associate Editor for the *European Transactions on Telecommunications* and an IEEE Senior member. She was Technical Program Committee Chair of AUSCTW'11, Melbourne, Australia. She was the Publicity Chair at the IEEE Information Theory Workshop 2009, Sicily, Italy. She is a Technical Program Committee member for various IEEE conferences such as IEEE ICC 2011, VTC 2011, PIMRC and WCNC 2008. Her research interests include information and communication theory with applications to telecommunication engineering.

Emanuele Viterbo was born in Torino, Italy, in 1966. He received his degree (Laurea) in Electrical Engineering in 1989 and his Ph.D. in 1995 in Electrical Engineering, both from the Politecnico di Torino, Torino, Italy. From 1990 to 1992 he was with the European Patent Office, The Hague, The Netherlands, as a patent examiner in the field of dynamic recording and error-control coding. Between 1995 and 1997 he held a post-doctoral position in the Dipartimento di Elettronica of the Politecnico di Torino. In 1997-98 he was a post-doctoral research fellow in the Information Sciences Research Center of AT&T Research, Florham Park, NJ, USA. He became first Assistant Professor (1998) then Associate Professor (2005) in Dipartimento di Elettronica at Politecnico di Torino. In 2006 he became Full Professor in DEIS at University of Calabria, Italy. Since September 2010 he is Full Professor in the ECSE Department and Associate Dean in Research Training at Monash University, Melbourne, Australia.

Prof. Emanuele Viterbo is an ISI Highly Cited Researcher since 2009. He is Associate Editor of IEEE TRANSACTIONS ON INFORMATION THEORY, *European Transactions on Telecommunications* and *Journal of Communications and Networks,* and Guest Editor for IEEE JOURNAL ON SELECTED TOPICS IN SIGNAL PROCESSING, Special Issue Managing Complexity in Multiuser MIMO Systems.

In 1993 he was visiting researcher in the Communications Department of DLR, Oberpfaffenhofen, Germany. In 1994 and 1995 he was visiting the Ecole Nationale Supérieure des Télécommunications (E.N.S.T.), Paris. In 2003 he was visiting researcher at the Maths Department of EPFL, Lausanne, Switzerland. In 2004 he was visiting researcher at the Telecommunications Department of UNICAMP, Campinas, Brazil. In 2005, 2006 and 2009 he was visiting researcher at the ITR of UniSA, Adelaide, Australia. In 2007 he was visiting fellow at the Nokia Research Center, Helsinki, Finland.

Dr. Emanuele Viterbo was awarded a NATO Advanced Fellowship in 1997 from the Italian National Research Council. His main research interests are in lattice codes for the Gaussian and fading channels, algebraic coding theory, algebraic space-time coding, digital terrestrial television broadcasting, digital magnetic recording, and irregular sampling.